A Numerical Study of Fluid-Solid Interaction
in Screw Compressors

Ahmed Kovacevic, University Research Fellow

Nikola Stosic, Chair in positive Displacement Technology

Ian K. Smith, Professor of Applied Thermodynamics

Centre for Positive Displacement Compressor Technology

City University, London EC1V 0HB, UK; Tel: +44 20 7040 8780; Fax: +44 20 7040 8566

e-mail: a.kovacevic@city.ac.uk

ABSTRACT

Efforts are continually being made to produce screw compressors with smaller clearances in order to reduce internal leakage. However, since the compression process induces large pressure differences across the rotors and temperature rise, they deform. A reliable method of estimating the interaction between fluid flow parameters and rotor deflection is thus needed in order to minimise clearances while avoiding contact between the rotors and the casing. A 3-D mathematical procedure is presented here to generate a numerical grid comprising both solid and fluid domains. This can be used to calculate the fluid flow and compressor structural deformation simultaneously by means of a suitable commercial numerical solver. Simulation results demonstrate the effects of change in working clearances, caused by rotor deformation, on compressor performance.

Keywords: Fluid–Solid Interaction, Screw Compressor, Analytical grid generation, Numerical simulation

NOTATION

ρ - density
p - pressure
T - temperature
m - mass
V - cell volume
t - time
T - stress tensor
S - viscous part of the stress tensor
v - velocity
u - deformation
μ, μ_t – molecular and turbulent viscosity
κ - thermal conductivity

h - enthalpy
c_i - concentration of species
k - turbulent kinetic energy
P - production of turbulence energy
ε - dissipation of turbulent kinetic energy
C, σ - constants in k-ε model of turbulence
Γ_ϕ – diffusion coefficient
$\mathbf{q}_{\phi S}, q_{\phi V}$ – source terms in transport equations

INTRODUCTION

Screw compressors comprise a meshing pair of helical rotors on parallel axes, contained in a casing. Together, they form a succession of working chambers whose volume depends on the angle of rotation. An outline of the main elements of a screw compressor is presented in Figure 1, where it is shown, by means of views from opposite ends and sides of the machine shows how the rotors are contained in the casing. The dark shaded portions show the enclosed region where the rotors are surrounded by the casing and compression takes place, while the light shaded areas show the regions of the rotors that are exposed to external pressure. The large light shaded area in Figure 1a) corresponds to the low pressure suction port. The small light shaded region between shaft ends B and D in Figure 1b) corresponds to the high pressure discharge port. Gas to be compressed enters the passages formed between the rotors and the casing through the low pressure port. After a certain angle of rotation, these are cut off from the port. Further rotation leads to a progressive reduction in the trapped volume which causes the pressure of the contained gas to rise. The compression process continues until the rear ends of the passages are exposed to the high pressure discharge port. Gas then flows out at approximately constant pressure as continuing rotation reduces the space between the rotors virtually to zero. The design parameter which influences screw compressor performance most strongly is the rotor profile. A difference in shape, which can hardly be detected by the eye, can effect significant changes in flow rates delivered and power consumption. Clearances between the rotors and between the rotors and the casing determine the leakage through the compressor and hence strongly influence both the volume flow rate and the power consumption.

Modern machine tools for rotor manufacturing enable screw compressor rotors to be produced at an economic cost with tolerances as small as 5 micrometers while casing bores can be manufactured on NC machine tools with a repeatability of 2 micrometers. Accordingly it is possible to construct compressors with very small clearances. Thus, internal leakages have been reduced to a fraction of their values in earlier designs. However, pressure changes in the passages due to compressor operation create loads on the rotors which make them bend and deform. This increases clearances between the rotors in areas where the pressure difference is the highest. Accordingly, internal leakage is the greatest in these regions. Therefore, rotor deflection is a significant parameter influencing compressor efficiency.

Dimensionless or quasi-steady mathematical models predict the overall effects of changes in the main design parameters on compressor overall behaviour fairly accurately. However, some effects cannot be taken into account by these models, especially if the influence of the local change in clearances caused by deformations induced by pressure and temperature fields in fluid is considered. Consequently, the simplified analytical models currently in use are not sufficiently accurate to design screw compressors to obtain the maximum possible improvements.

A full 3-D numerical calculation of the compressor fluid flow and solid structure is therefore required to determine the maximum reduction in clearances possible to improve screw compressor performance without contact between the rotors and their casing. By this means, rotors may be manufactured with minimum working clearances and screw compressors may be made smaller as well as more efficient.

A Computational Continuum Mechanics (CCM) method simultaneously combines and solves the fluid flow and structure behaviour to determine the effects of changes in the compressor geometry on internal heat and fluid flow and vice versa. Such an approach can produce reliable predictions only if calculated over a substantial number of grid points. Hence, a high computer potential and capacity is needed in order to use such procedures to analyse a screw compressor.

Apart from the authors' publications, *Kovacevic et. al.* [3] - [6], there are hardly other reported activities in the use of CFD for screw compressor studies. This is mainly because the existing grid generators and the majority of solvers are still unable to cope with the problems associated with both the screw compressor geometry and the physics of the compressor process. Also, difficulties in obtaining simultaneous calculation for solid and fluid domains in order to evaluate fluid-solid interaction have contributed to the lack of publications in this area.

Based on successful application of finite volume calculations of 3-D flows to complex curvilinear geometries, *Ferziger and Peric* [2] published a book on finite volume methods for fluid dynamics. *Demirdzic and Muzaferija* [1] showed a possibility of simultaneous application of the same numerical methods in fluid flow and structural analysis within moving frames on structured and unstructured grids.

A number of authors have discussed contemporary grid generation methods extensively. The most detailed textbooks in that area are *Liseikin* [7] and *Thompson* et al [11]. Adequately applied, the grid generation they describe, accompanied by an appropriate CCM solver, leads to the successful prediction of screw compressor fluid-solid interaction. Such an approach results in an algebraic grid generation method, which employs a multi parameter adaptation. The authors give this in detail in *Kovacevic et al* [4]. They also describe an interface, which transfers the screw compressor geometry to a CFD solver and compressor suction flow is given as a working example. The interface employs a rack generation procedure to produce rotor profile points and analytical transfinite interpolation between them with adaptive meshing to obtain a fully structured 3-D numerical mesh. This grid is directly transferable to a CFD code. Some changes needed be made within the solver functions to enable accurate and faster calculations. These include a means to maintain constant pressure at the inlet and outlet ports and interaction between solid and fluid domains.

To apply simultaneous calculations of the solid structure and fluid flow, changes have to be made in the grid generation procedure to allow for grid generation of both, solid compressor elements and fluid flow areas. A procedure for adaptive representation of an interface between the solid and fluid

finite volumes is described in this paper that enables accurate and conservative calculation of the interaction between fluid flow and solid body deformation. This is calculated by use of general mass averaged equations of continuity, fluid and solid momentum, energy, concentration and space conservation. These are accompanied by Stoke's law for the fluid domains and Hooke's law for the solid compressor domains. By this means, distortions of the solid body domains are automatically accounted for in the fluid flow passage geometry. These then cause changes of velocity, temperature, pressure and density in the fluid domain.

GRID GENERATION FOR FLUID SOLID INTERACTION

The grid generation of screw compressor geometry is a necessary preliminary to the CCM calculation. Firstly, it defines spatial domains that represent the metal material inside the rotors and the fluid passages outside the rotors. These are determined by the rotor profile coordinates and their derivatives and are obtained by means of the rack generation procedure described in detail by *Stosic* [9].

By use of the methods of *Liseikin* [7] and *Thompson et al* [11], already mentioned, an algebraic grid generation method for screw compressor fluid flow was derived, based on a transfinite interpolation procedure. This includes stretching functions to ensure grid orthogonality and smoothness, as described by the authors in Kova*cevic et al*, [6]. In that case, the compressor spatial domain is divided in a number of sub-domains, which allow generation of a fully structured numerical grid of discrete volumes. A composite grid is then made of several blocks patched together and based on a single boundary fitted co-ordinate system. Block structured grids allow easier mapping for complex geometries. Two basic block topologies are used for screw compressor grid generation, namely polyhedral blocks a) and "O" grids b) as presented in Figure 2.

A feature associated with the interaction of the fluid flow and solid structure is that the numerical grid for both, the fluid around the rotors and the rotors themselves is generated simultaneously in a single, fully structured block. This allows distortions to change the interlobe, radial and end clearances and accounts for them in the fluid flow calculation. A number of points required in this case to define the rotor geometry accurately is generally not very large. However, if a sliding interface between the solid and fluid is applied, a number of points needed may be too large that a numerical mesh, so formed cannot be used. One means of resolving this problem, which combines accuracy with fast solution, is to keep the number of computational cells as low as possible and to modify a distribution of points according to the local requirements. An additional reason for this approach is that the principal dimension of the screw compressor chamber may vary from as little as 30 micrometers to tens of millimetres. It is therefore not unusual for a grid length scale ratio to exceed 500. Since the number of cells in the radial direction is kept constant throughout the compressor solid section, as well as in the flow chamber and in the gaps, the ratio between the circumferential and radial dimensions of

the cell can easily become unacceptable. However, the same number of cells can form a suitable grid if the boundary is adapted carefully to keep the grid aspect ratio as uniform as possible.

An equidistribution procedure is therefore applied to the boundary regions between the rotor and its fluid domain. It requires the product of the grid spacing and a 'weight function' to be constant. The weight function is based on an adaptation variable, which can be selected according to geometry requirements. The adaptation procedure is carried out in four major steps; namely: a) selection of adaptation variables, b) evaluation of integral adaptation functions, c) calculation of new transformed coordinate and d) obtaining new physical coordinate by inverse interpolation.

Once a satisfactory point distribution on the rotor boundary is achieved, the distribution of points on the opposite sliding interface boundary, must be obtained for convenient generation of the numerical points in the interior of the domain. That boundary is mapped with the same number of points as the previous one so the cells that are formed from the appropriate nodes on both boundaries are always regular. For that reason, a special procedure was developed to transform the physical domain into a simplified computational domain in which the adaptation is performed.

NUMERICAL SOLUTION OF THE FLUID-SOLID INTERACTION

The density of the compressor working fluid changes with both pressure and temperature. The compressor flow and the structure of compressor parts is fully described by the mass averaged conservation equations of continuity, momentum, energy and space, which are accompanied by the turbulence model equations and an equation of state, as it is, for example, explained by *Ferziger and Peric* [2]. In the case of multiphase flow, a concentration equation is added to the system. The numerical solution of such a system of partial differential equations is then made possible by inclusion of constitutive relations in the form of Stoke's, Fick's and Fourier's law for the fluid momentum, concentration and energy equations respectively and Hooke's law for the momentum equations of a thermo-elastic solid body.

All these equations are conveniently written in a form of the following generic transport equation:

$$\frac{d}{dt}\int_V \rho\phi dV + \int_S \rho\phi(\mathbf{v}-\mathbf{v}_s)\cdot d\mathbf{s} = \int_S \Gamma_\phi \operatorname{grad}\phi\cdot d\mathbf{s} + \int_S \mathbf{q}_{\phi S}\cdot ds + \int_V q_{\phi V}\cdot dV \qquad (1)$$

Here ϕ stands for the transported variable and Γ_ϕ is diffusion coefficient. The meaning of source terms, $\mathbf{q}_{\phi S}$ and $q_{\phi V}$ for the fluid and solid transport equations is given in Table 1.

The resulting system of partial differential equations is discretised by means of a finite volume method in the general Cartesian coordinate frame. This method enhances the conservation of governing equations while at the same time enables a coupled system of equations to be solved simultaneously for both the solid and fluid regions.

Table 1 Terms in the generic transport equation (1)

Equation	ϕ	Γ_ϕ	$\mathbf{q}_{\phi S}$	$q_{\phi V}$
Fluid Momentum	v_i	μ_{eff}	$\left[\mu_{eff}\left(\text{grad }\mathbf{v}\right)^{\text{T}} - \left(\dfrac{2}{3}\mu_{eff}\text{div }\mathbf{v} + p\right)\mathbf{I}\right]\cdot\mathbf{i}_i$	$f_{\text{b},i}$
Solid Momentum	$\dfrac{\partial u_i}{\partial t}$	η	$\left[\eta\left(\text{grad }\mathbf{u}\right)^{\text{T}} + \left(\lambda\text{div }\mathbf{u} - 3K\alpha\Delta T\right)\mathbf{I}\right]\cdot\mathbf{i}_i$	$f_{\text{b},i}$
Energy	e	$\dfrac{k}{\partial e/\partial T} + \dfrac{\mu_t}{\sigma_T}$	$-\dfrac{k}{\partial e/\partial T}\dfrac{\partial e}{\partial p}\cdot\text{grad}p$	$\mathbf{T}:\text{grad }\mathbf{v} + h$
Concentration	c_i	$\rho D_{i,\text{eff}}$	0	s_{ci}
Space	$\dfrac{1}{\rho}$	0	0	0
Turbulent kinetic energy	K	$\mu + \dfrac{\mu_t}{\sigma_k}$	0	$P - \rho\varepsilon$
Dissipation	ε	$\mu + \dfrac{\mu_t}{\sigma_\varepsilon}$		$C_1 P\dfrac{\varepsilon}{k} - C_2\rho\dfrac{\varepsilon^2}{k} - C_3\rho\varepsilon\,\text{div }\mathbf{v}$

This mathematical scheme is accompanied by boundary conditions for both the solid and fluid parts. A special treatment of the compressor fluid boundaries has been introduced by *Kovacevic et al* [5]. The compressor was positioned between the two relatively small suction and discharge receivers. By this means, the compressor system is separated from the surroundings by adiabatic walls only. It communicates with its surroundings through the mass and energy sources or sinks placed in these receivers to maintain constant suction and discharge pressures. The solid part of the system is constrained by both Dirichlet and Neuman boundary conditions through zero displacement in the restraints and zero tractions elsewhere. Connection between the solid and fluid parts is determined explicitly if the temperature and displacement from the solid body surface are boundary conditions for the fluid flow and vice versa.

The numerical grid was applied to a commercial CCM solver to obtain distribution of pressure, temperature, velocity and density fields throughout the fluid domain as well as deformations and stresses of the solid compressor elements. Based on the solution of these equations, integral parameters of screw compressor performance were calculated, *Kovacevic et. al.* [6], *Stosic et. al.* [10].

PRESENTATION AND DISCUSSION OF THE RESULTS

The interaction between fluid flow and solid parts is analysed in this paper for an oil-injected air screw compressor shown in Figure 3. The Rotor profiles are of the 'N' type with a 5/6 lobe configuration, as presented in *Stosic et. al.* [8]. The rotor outer diameters are 128 and 101 mm for the male and female rotors respectively, and their centre distance is 90 mm. The rotor length to diameter

ratio is 1.65. A numerical mesh for the test case in this study comprises 513,617 numerical cells of which 162,283 cells represent the solid part of the rotors, 189,144 other cells are mapped on the fluid parts between the rotors while the rest are numerical cells of the suction and discharge domains which include both, the suction and discharge ports and oil openings. A cross section through the numerical mesh for rotors and their fluid paths is presented in Figure 4.

Grid and other control parameters generated by the interface were applied to Comet, a commercial CMM solver of StarCD. The results obtained are presented in this paper for three different applications, namely, for an oil-injected air compressor of moderate pressure ratio, a dry air compressor, in which the pressure ratio is low, due to discharge temperature restrictions, and a high pressure oil flooded compressor. The calculations were carried out on a computer powered by an Athlon 800 MHz processor and 1 GB memory. Compressor rotation was simulated by means of 24 time steps for one interlobe rotation. This was equivalent to 120 time steps for one full rotation of the male rotor. The time step length was synchronised with a compressor speed of 5000 rpm. Error reduction of 4 orders of magnitude was required, and achieved for approximately 50 outer iterations at each time step, which took approximately 30 minutes of computer time for one time step. The overall compressor parameters such as torque, volume flow, forces, efficiencies and compressor specific power were then calculated. Additionally, pressure-time diagrams of the compression process, the flow and pressure patterns in the compressor chambers and rotor deformation are provided.

The measurements were also performed for one of the modelled compressors. Pressure fluctuations in the experimental compressor are measured by piezoresitive transducers conveniently positioned in the compressor housing at the male rotor side to cover as much as possible of the compressor process. In the case of the oil injected air compressor, the measured results were compared with those obtained from numerical simulations, for a suction pressure of 1 bar and discharge pressures of 6, 7, 8 and 9 bar and the results are shown in Figure 5. Good agreement was obtained both for the instantaneous values and integral parameters, as shown in Figure 6.

Screw compressor rotors are deformed both by the fluid pressure loads in the machine and temperature distortions of the solid body. The latter are caused by temperature rise in the compression chamber. Therefore, three cases are considered and compared here which correspond to three the most usually used compressor types.

In case 1, the oil flooded air compressor works between 1 bar and 20 $^{\circ}$C suction and 7 bar discharge. A substantial amount of oil was injected in the compressor in order to keep the discharge temperature as low as possible. The average temperature at the compressor exit of 40 $^{\circ}$C was retained throughout the compressor working cycle. Consequently, rotor deformation was caused mainly by the pressure field in the compressor working chamber. Two views of the rotors for that condition are presented in Figure 7, one from the bottom of the rotors and the other one from the female rotor side.

Pressure forces push the rotors apart and bend them in the space, which is visible from the top diagram. By this means, the leakage path through the sealing line between the rotors is biggest on the discharge side where the pressure ratio between the two rotor sides is the greatest. Also, rotor bending increases the clearance gap between the rotor and the housing on the discharge side of the compressor. The female rotor is weaker then the male one and therefore it is deformed more. The highest recorded deformation in this case was in the range of few micrometers. In order to visualise the rotors in the deformed state, the distortion has been magnified 20,000 times while other physical and geometrical values are kept at their original scale.

Case 2 is an oil free air compressor of the same rotor and housing arrangement as in the Case 1. The compressor works between the suction conditions of 1 bar and 20 ^{o}C and a discharge pressure of 3 bar. Due to the lack of oil cooling, a temperature rise in the compressor is much greater and has an average value of 150 ^{o}C at the discharge port. Such working conditions cause completely different deformations then in the Case 1. These are presented in Figure 8. The deformations caused by the pressure difference are negligible compared to the deformations cause by the temperature change. Fluid temperature in the immediate vicinity of the solid boundary changes rapidly as shown in the bottom diagram. However, the temperature of a rotor pair is lower due to the continuous averaging oscillations of pressure and temperature in the neighbouring fluid. This is shown in the top diagram, Figure 8 where the temperature distribution is given in a cross section for both the fluid flow and the rotor body. The deformations presented in the bottom of the figure show the enlargement of the rotors in the discharge area. These deformations are more than an order of magnitude higher then in the case of the oil flooded compressor. They reached 50μm in the discharge section of the rotors and thus reduce the rotor working clearances by the same amount. By this means leakage flow in the most critical areas is reduced. However, in the design of the dry screw compressor, sufficient initial clearance should be allowed to prevent rotor seizure caused by temperature distortions. The deformations are scaled 1,500 times in order to visualise them in Figure 8.

Case 3 represents a high pressure oil injected compressor. The example is given here for a CO_2 compressor with suction conditions of 30 bar and 0°C and a discharge pressure of 90 bar. The discharge temperature was 40 ^{o}C. In this case, the large pressure difference caused higher rotor deflections than in the Case 1, as shown in Figure 9. The highest deformation was in excess of 15μm, which is the same order of magnitude as it was found in the case where temperature deformation was dominant. The deformation pattern of the rotors is similar to that in the Case 1 but only slightly enlarged at the discharge side.

The influence of the rotor deformation to the integral screw compressor parameters caused by the change in clearance is given in Figure 10. The reduction of rotor clearances due to the enlargement of the rotors caused by temperature dilatations results in an increase in both, the compressor flow and power input. However the flow increase is relatively larger than that of the power and hence results in

a decrease in specific power, or more conventionally, an increase in efficiency, as shown in the diagram. for the other cases, the rotor deflections caused by the pressure enlarge the clearances. For a moderate compressor pressure, the clearances gap is enlarged only slightly and hence has only a negligible influence on the delivery and power consumption. In the case of high working pressures as, for example, in CO_2 a refrigeration application, the rotors deform more and the decrease in the delivery and rise in specific power becomes more pronounced.

CONCLUSIONS

Screw compressor elements, especially their rotors are heavily loaded by pressure forces and are subjected to temperature distortions. These cause the rotors to deform during normal operation. The working clearances therefore vary and become smaller or larger, thereby affecting the internal leakage. This usually leads to deterioration in the compressor performance. A full 3-D calculation has been performed to quantify the interaction of the compressor structure and compressor fluid flow. The effects of the change in working clearances are compared for different compressor applications and presented through distortion diagrams and flow-power charts. As is shown in the results, the rotor deformation is dependent on the compressor application. It must, therefore, be taken into account in every specific compressor design.

REFERENCES

1. Demirdzic, I., Muzaferija S., "Numerical Method for Coupled Fluid Flow, Heat Transfer and Stress Analysis Using Unstructured Moving Mesh with Cells of Arbitrary Topology", Comp. Methods Appl. Mech Eng, 1995, Vol. 125, pp 235-255
2. Ferziger, J.H., Peric, M.; "Computational Methods for Fluid Dynamics", Springer, Berlin, Germany, 1996
3. Kovacevic, A.; Stosic, N.; Smith, I.K.; "The CFD Analysis of a Screw Compressor Suction Flow", 2000 International Compressor Conference at Purdue University, West Lafayette, Indiana, July 2000, pp 909-916
4. Kovacevic, A., Stosic, N.; Smith, I.K.; "Grid Aspects of Screw Compressor Flow Calculations", Proceedings of the ASME International Mechanical Engineering Congress, Orlando, Florida, November 2000, pp 79-82
5. Kovacevic, A.; Stosic, N.; Smith, I.K.; "Analysis of Screw Compressor by Means of Three-Dimensional Numerical Modelling", International Conference on Compressor and their System, IMechE Conference Transactions 2001-7, London, 2001, p.23-32
6. Kovacevic, A.; Stosic, N.; Smith, I.K.; "CFD Analysis of Screw Compressor Performance ", In: "Advances of CFD in Fluid Machinery Design" edited by Elder, R.L, Tourlidakis, A, Yates M.K, Professional Engineering Publishing of ImechE, London, 2002
7. Liseikin, V.D., "Grid generation Methods", Springer-Verlag, 1999
8. Stosic, N.; Smith, I.K.; Kovacevic; A, Aldis C.A., "The Design of a twin-screw compressor based on a new rotor profile", Journal of Engineering Design, v.8, n.4 1997, pp 389-399
9. Stosic, N.; "On Gearing of Helical Screw Compressor Rotors", Proc IMechE, Journal of Mechanical Engineering Science, 1998, Vol.212, pp 587
10. Stosic, N, Hanjalic K., "Development and Optimization of Screw Machines with a Simulation Model, Part I: Profile Generation, Part II: Thermodynamic Performance Simulation and Design", ASME Proceedings, Journal of Fluids Engineering,1997, Vol 119, p 659, p664
11. Thompson, J.F; Soni, B.; Weatherrill, N.P.; "Handbook of Grid generation", CRC Press 1999
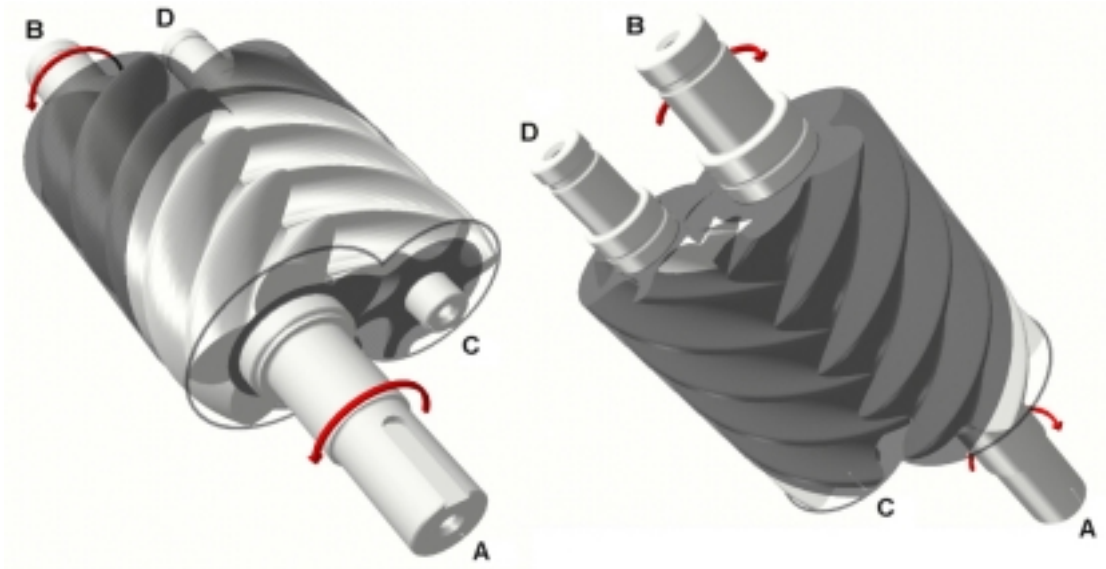
a) Top Front View   b) Bottom Rear View

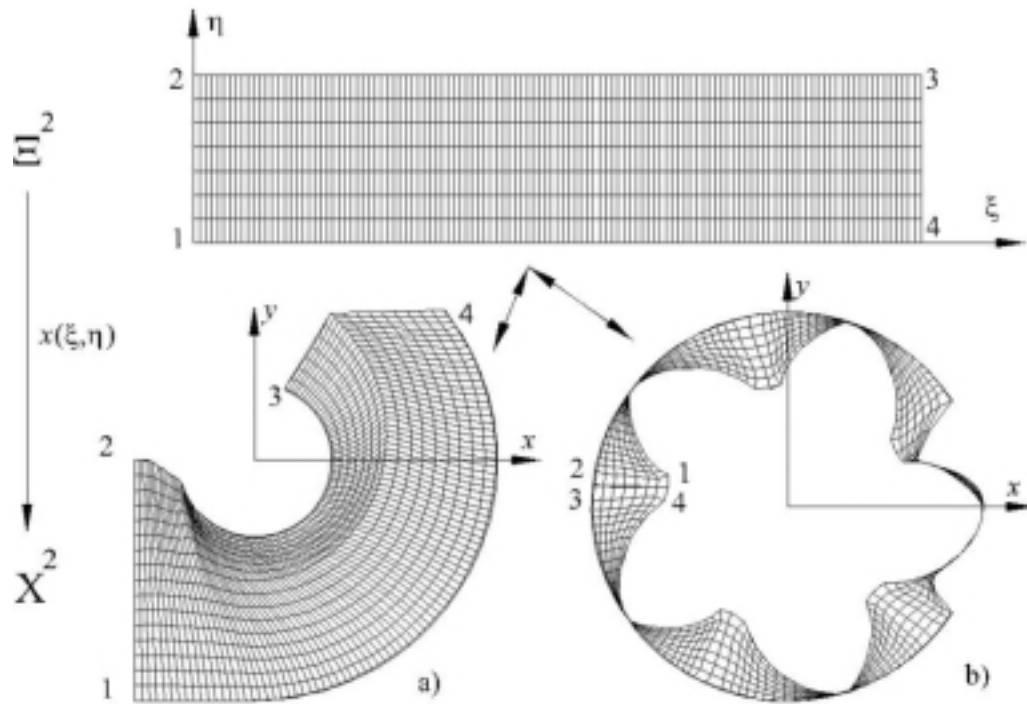*Figure 1 Twin Screw Compressor Rotors and Casing Outline*

Figure 2 Types of numerical grids used for definition of screw compressor geometry
a) polyhedral grid,   b) "O" grid

Main Rotor: RH
Lead 238.579 mm
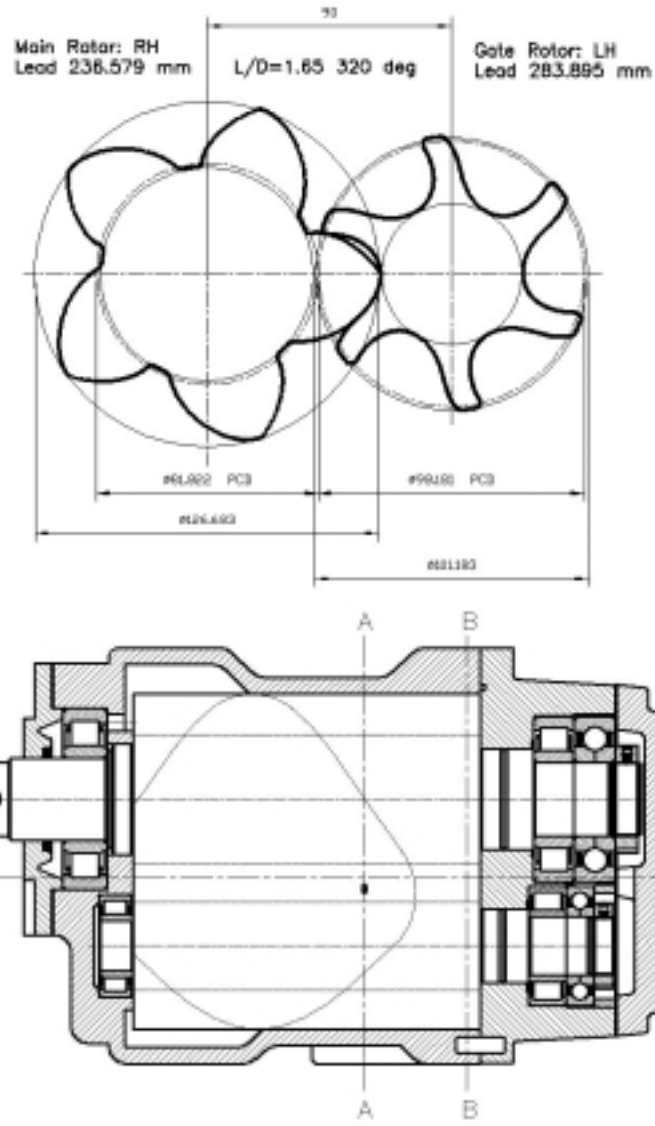
L/D=1.65 320 deg

Gate Rotor: LH
Lead 283.895 mm

Figure 3 Cross section of rotors (top) and compressor (bottom)
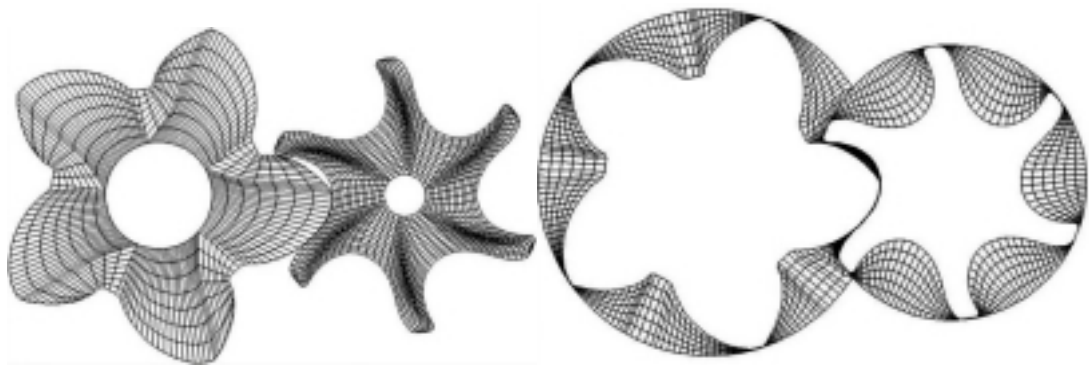
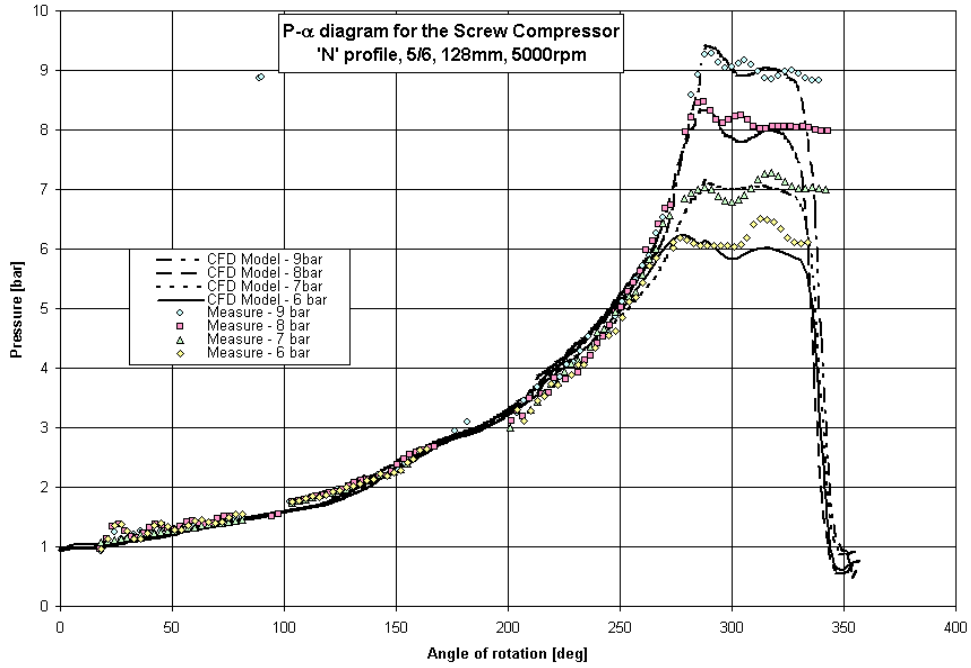*Figure 4 Numerical mesh for rotors (left) and their fluid parts (right)*

Figure 5 Pressure-shaft angle diagram; comparison of CFD calculations and measurements
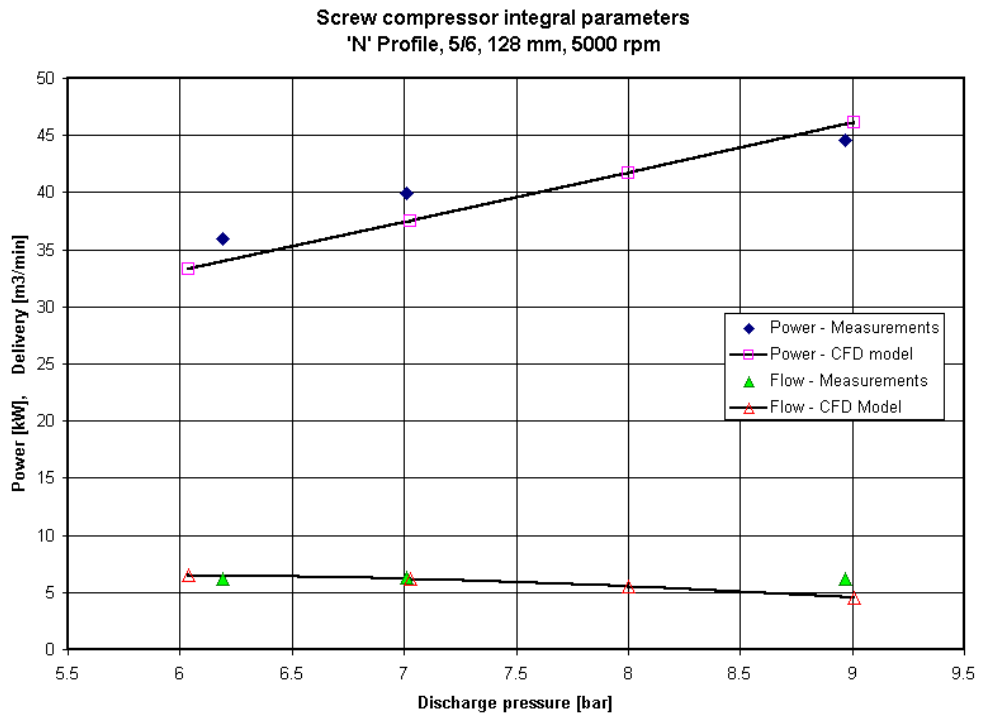
Figure 6 Comparison of integral results obtained by measurements and modelling
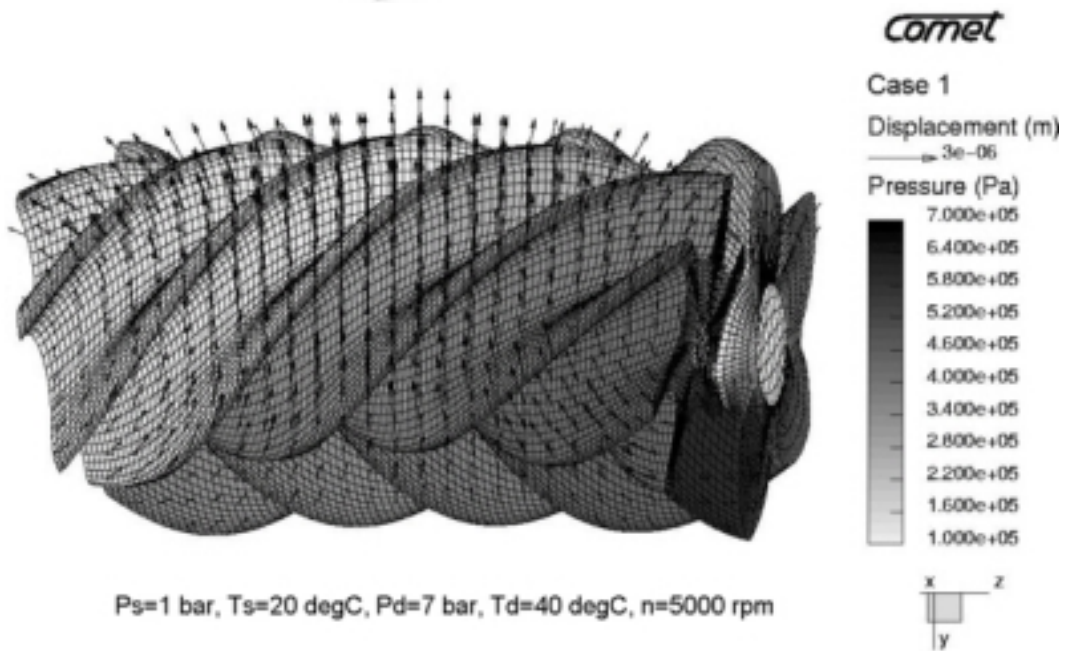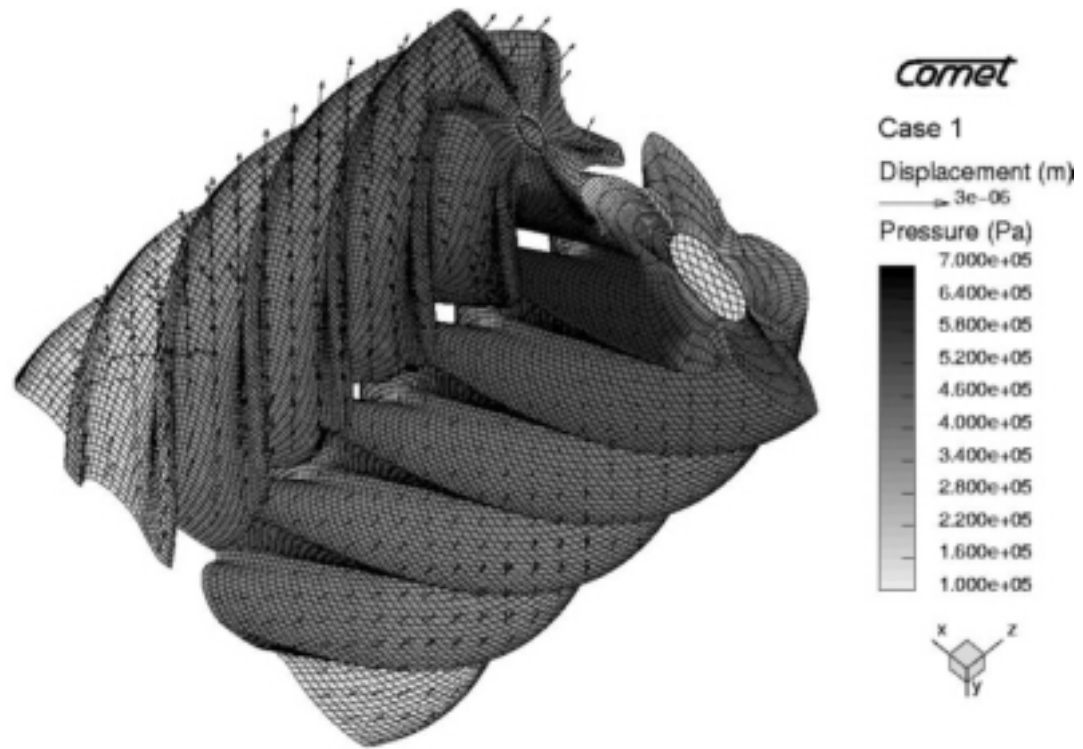
Figure 7 Displacement vectors and the acting pressure on deformed rotors for oil injected compressor
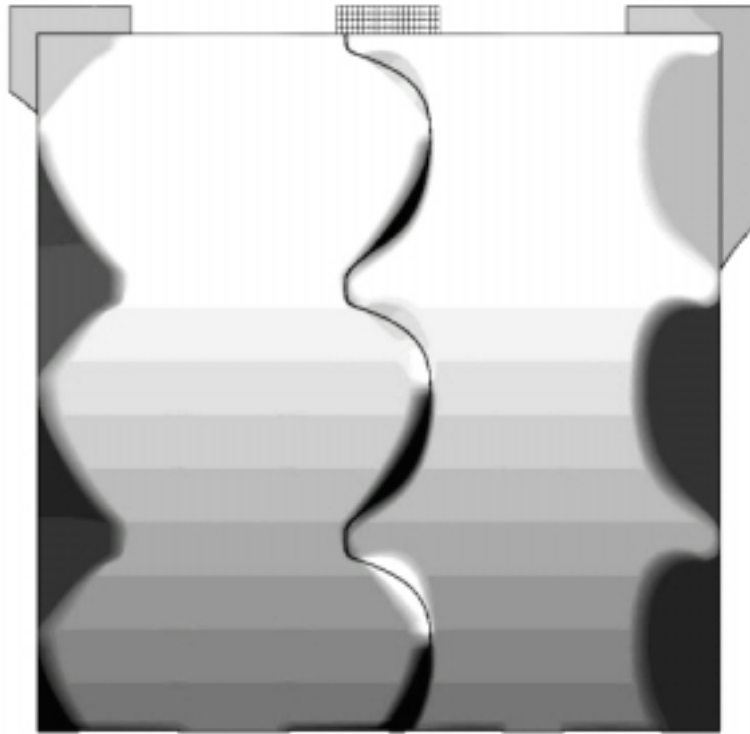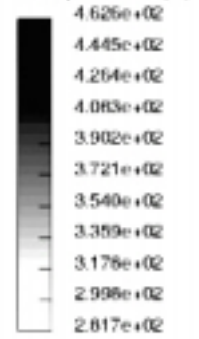
Ps=1 bar, Ts= 20 degC, Pd=3 bar, Td=150 degC, n=5000 rpm
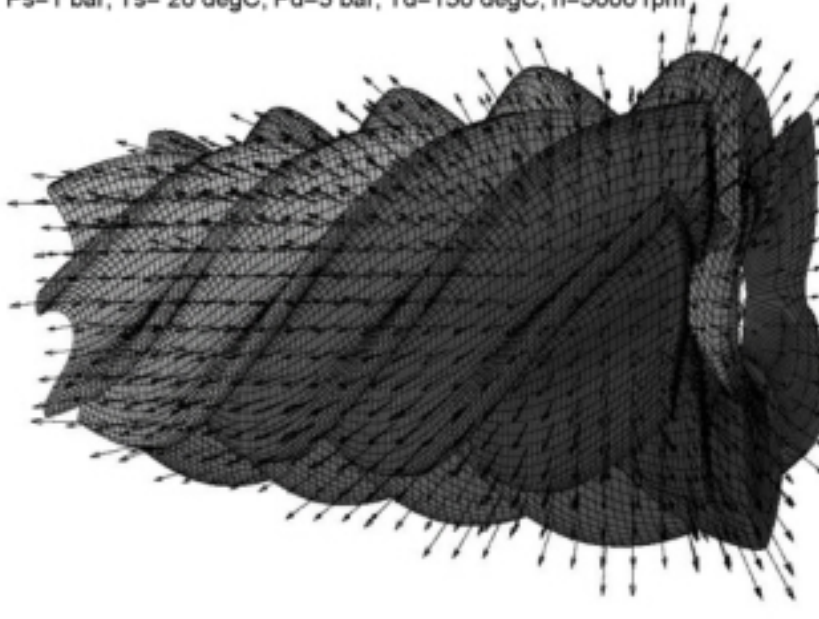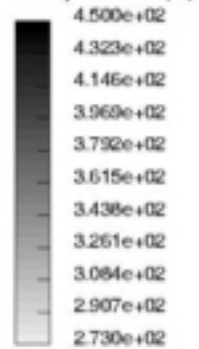
Figure 8 Rotor displacement vectors and temperature distribution for an oil free compressor

Ps=30 bar, Ts= 0 degC, Pd=90 bar, Td=40 degC, n=5000 rpm
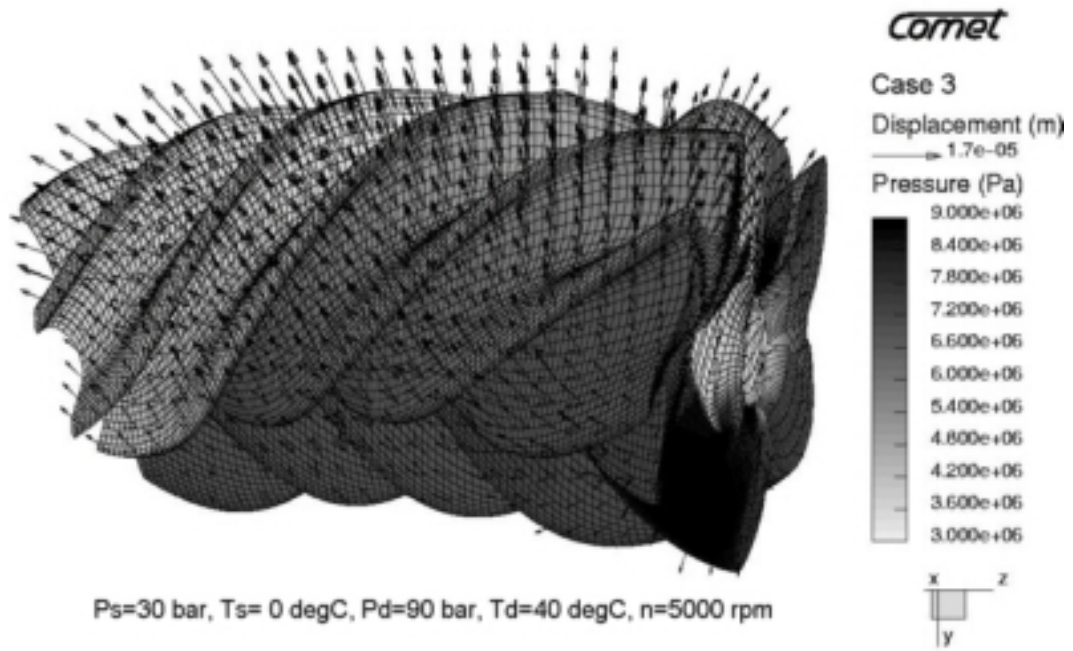
Figure 9 Deformations of a high pressure oil injected compressor

Screw compressor integral parameters
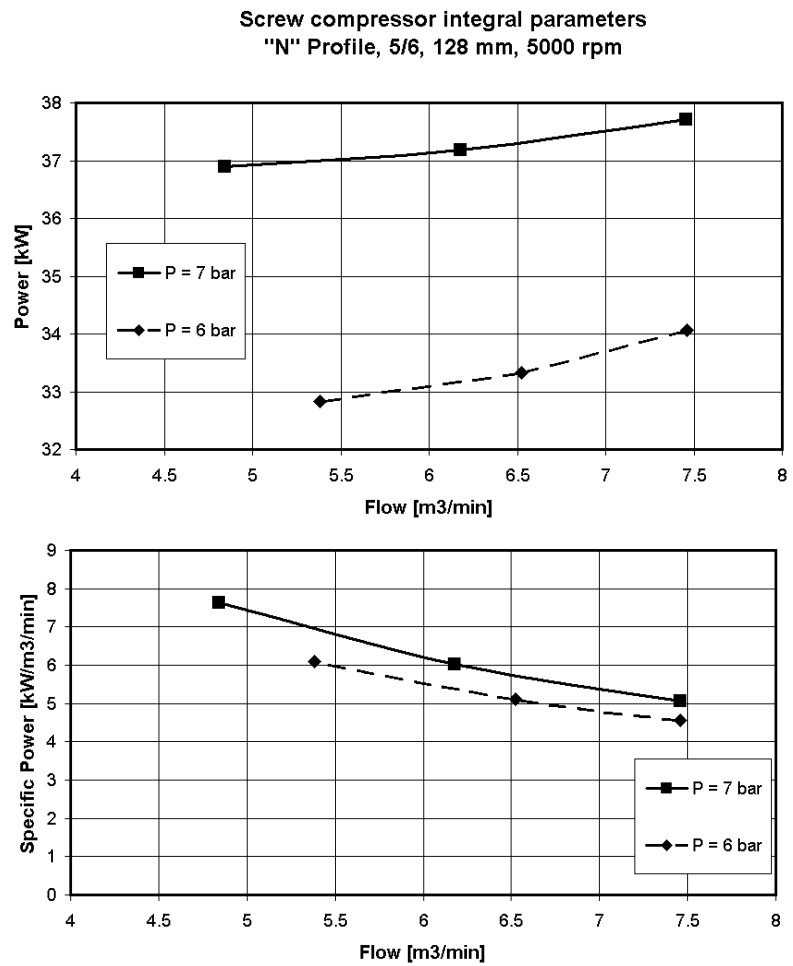**"N" Profile, 5/6, 128 mm, 5000 rpm**

Figure 10 Influence of the rotor deflection to the integral compressor parameters